Journal of Hydrology 436–437 (2012) 35–50

Contents lists available at SciVerse ScienceDirect

Journal of Hydrology

journal homepage: www.elsevier.com/locate/jhydrol

Roots, storms and soil pores: Incorporating key ecohydrological processes into Budyko's hydrological model

Randall J. Donohue [a,*], Michael L. Roderick [b], Tim R. McVicar [a]

[a] CSIRO Land and Water, GPO Box 1666, Canberra, ACT 2601, Australia
[b] Research School of Biology and Research School of Earth Sciences, The Australian National University, Canberra, ACT 0200, Australia

ARTICLE INFO

Article history:
Received 21 September 2011
Received in revised form 15 February 2012
Accepted 16 February 2012
Available online 25 February 2012
This manuscript was handled by
Geoff Syme, Editor-in-Chief

Keywords:
Choudhury
Porporato
BCP model
Rooting depth
Storm depth
Seasonality

SUMMARY

Due to its role in intercepting and evaporating water, vegetation is a key medium through which catchment water yields can be manipulated and may prove to be an important tool available to managers for mitigating the effects of climatic changes on yields. Understanding of the effects of vegetation on long-term catchment flows is growing, yet incorporation of these effects into hydrological models has typically been empirical and qualitative, or deterministic and quantitative – but at the cost of simplicity. Here we present a new ecohydrological model (the Budyko–Choudhury–Porporato, or BCP, model) that is the combination of two pre-existing models. It is simple, quantitative and process-based. As well as accounting for the well established roles played by average precipitation (P) and potential evaporation (E_p) on long-term catchment flows (R), the BCP model also provides estimates of n – a catchment-specific model parameter that alters the partitioning of P between R and evaporation – which is estimated as a function of plant-available soil water holding capacity (κ), mean storm depth (α) and effective rooting depth (Z_e).

After developing this model and testing results at several spatial scales across Australia, we used the model to analyse the sensitivity of R to changes in Z_e and α (as well as P and E_p) in the high yield zones of the Murray-Darling Basin. The model performed well overall at both the coarse spatial scale (i.e., the Basin) and at the finer scales of sub-basin regions and of catchments, capturing ~90% of the observed variability in R. At the regional scale, BCP-modelled R was more or less the same as when a default (constant) value of n was used to model R (that is, $n = 1.8$). This is due to the general aridity of these regions (under such conditions R is insensitive to small variations in n). However, at the catchment scale, use of the BCP model in 'wet' catchments (i.e., $R > 500$ mm y^{-1}) increased the accuracy of predictions by approximately 10% compared to the default ($n = 1.8$) model.

Runoff was shown to be highly sensitive to changes in P in the highest yield zones of the Basin, followed by changes in Z_e and then in α. In contrast, across the whole basin – which is highly arid – the sensitivity of R to changes in Z_e and α, whilst small in absolute terms, are substantial relative to total basin flows. The incorporation of α, κ and – most importantly from a management perspective – Z_e into the Budyko model provides a simple and transparent tool for aiding the understanding of the long-term ecohydrological behaviour of catchments and assessing the potential hydrological effects of different land management options under a variable climate.

1. Introduction

What options are available to catchment managers for mitigating the effects of climate change on catchment water yields? Most climate-related processes lie outside the realm of everyday human control. On the other hand, many land surface characteristics influence the partitioning of precipitation into evaporation and runoff and these characteristics can be effectively managed – which essentially entails vegetation management. Vegetation affects precipitation interception rates, infiltration rates, soil water storage capacity and the rate of depletion of soil stores, each of which alter partitioning (Calder, 1993; Rodriguez-Iturbe and Porporato, 2004). An essential ability, then, for planning and management purposes is the capacity to assess the effects of changes in vegetation characteristics on runoff and, hence, on water yield.

In this paper we develop and test a simple ecohydrological model that quantifies the effects of changes in precipitation, potential evaporation, effective rooting depth, mean storm depth and soil water storage capacity on long-term average runoff. This model combines Choudhury's (1999) version of Budyko's (1974) hydrological model with Porporato et al.'s (2004) ecohydrological model. We utilise the runoff sensitivity framework presented by Roderick and Farquhar (2011) to assess the effects of changes in these

* Corresponding author. Tel.: +61 2 6246 5803.
E-mail address: Randall.Donohue@csiro.au (R.J. Donohue).

0022-1694/$ - see front matter © 2012 Elsevier B.V. All rights reserved.
http://dx.doi.org/10.1016/j.jhydrol.2012.02.033

ecohydrological variables on runoff. In addition, we build upon the work of Donohue et al. (2011) who applied the above sensitivity framework to Budyko-modelled runoff in a spatially explicit manner across the Murray-Darling Basin (MDB), in Australia, looking particularly at runoff dynamics of the high yield zones within the Basin.

The first aim of this paper is to combine the Choudhury and Porporato models in order to explicitly incorporate the impacts of soil water holding capacity, mean storm depth and effective rooting depth on long-term average stream flow. This combined Budyko–Choudhury–Porporato model (the 'BCP' model) enables n, a catchment specific parameter (Choudhury, 1999; Roderick and Farquhar, 2011; Yang et al., 2008), to be modelled spatially. We apply the BCP model across Australia, testing its performance at several spatial scales within the MDB. A significant aspect of developing the BCP model is to generate Australia-wide estimates of effective rooting depth. The second aim of this paper is to assess the sensitivity of runoff to changes in effective rooting depth and mean storm depth within the high water yielding zones of the MDB. Prior to describing the development of the BCP model and then applying it to the MDB, we next provide a brief background to the Budyko/Choudhury and Porporato models, to the sensitivity framework of Roderick and Farquhar, and to the ecohydrological characteristics of the MDB.

2. Background

2.1. Budyko's hydrological model and Choudhury's equation

Long-term average actual evaporation (E, mm y^{-1}) and runoff (R, mm y^{-1}) can be estimated using Budyko's (1974) hydrological model. This model estimates the evaporative index (ε) – the ratio between E and precipitation (P, mm y^{-1}) – as a non-linear function of the climatic dryness index (Φ) – the ratio of potential evaporation (E_p, mm y^{-1}) to P (Fig. 1). The utility of the Budyko model lies in its simplicity as it frames catchment processes in terms of energy and water supply–demand balances whilst maintaining the link between surface energy and water balances. It is also analytical and therefore highly transparent. Many useful generalisations about catchment behaviour can be made based on the degree of energy or water limitation. Several summaries and discussions of the Budyko model have been published (e.g., Donohue et al., 2007; Gerrits et al., 2009; Milly, 1994b; Roderick and Farquhar, 2011; Yang et al., 2006, 2008; Zhang et al., 2004). The works of Milly (1994b) and Gerrits et al. (2009), in particular, provide important insights into the processes that generate the characteristic 'Budyko curve', many of which relate to variability in the supplies of water and energy and in soil water storage capacity. A key aspect of the Budyko model is that it assumes hydrological steady state conditions and consequently is suitable only for examining the differences between two steady states as opposed to examining transitional states.

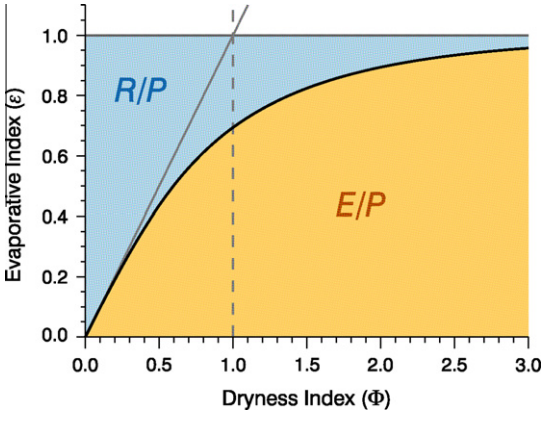

Fig. 1. The Budyko curve and the supply–demand framework. The Budyko curve (black line) describes the relation between ε and Φ. The horizontal grey line is the water-limit, where 100% of P becomes E, and the diagonal grey line is the energy-limit, where 100% of available evaporative energy (i.e., E_p) is converted to latent heat. The orange shaded area represents ε and the blue shaded area represents the fraction of P that becomes R. To the left of the dashed line are energy-limited conditions ($\phi < 1$) and to the right are water-limited conditions ($\phi > 1$). (For interpretation of the references to colour in this figure legend, the reader is referred to the web version of this article.)

Choudhury (1999) formulated the Budyko curve as

$$\varepsilon = \frac{E}{P} = \frac{R_n}{\left(P^n + R_n^n\right)^{1/n}}, \tag{1}$$

where n is the 'catchment properties parameter' that alters the partitioning of P between modelled E and R (although Choudhury used α instead of n). In Choudhury (1999) available energy was represented using net radiation (R_n; mm y^{-1}) however E_p is now more commonly used (e.g., Yang et al., 2008) – and will be used here. Under steady state conditions, the runoff is simply the difference between P and E,

$$R = P - E = P - \frac{PE_p}{\left(P^n + E_p^n\right)^{1/n}}. \tag{2}$$

Choudhury (1999) suggested using $n = 1.8$ for catchment-based studies and this is now a commonly used 'default' value. It is worth pointing out that this value for catchments was derived using R_n not E_p and, as average R_n is typically lower than E_p, an equivalent 'default' catchment value when E_p is used in the formulation will be higher than 1.8. This subtlety is generally ignored in practice. Donohue et al. (2011) showed that, when $\phi = 1$, the value of n that best reproduces the original Budyko curve is 1.9. Generally speaking, the catchment properties parameter, n, represents the net effect on R of any processes not already encapsulated in P and E_p (Zhang et al., 2004), including errors in the representation of P and E_p. Its relation to physical attributes remains obscure despite several specific investigations (Donohue et al., 2010b; Oudin et al., 2008; Peel et al., 2010; Yang et al., 2007, 2009; Zhang et al., 2001). Hence, there is currently no definitive process-based understanding of what determines n.

2.2. The ecohydrological model of Porporato and others

Functionally, effective rooting depth (Z_e, mm) and mean depth per storm event (α, mm) have complimentary effects on R as a large α, which produces a relatively large R, can be offset by a large Z_e, which produces a relatively low R, all else being equal (Milly, 1994b; Porporato et al., 2004). Whilst Z_e defines the total depth to which plant-accessible water can be stored (i.e., soil depth of storage), the fractional plant-available water holding capacity (κ; 0–1, dimensionless) defines the maximum depth of water that can be held within the total storage depth (i.e., water depth of storage). Porporato et al. (2004) incorporated the effects of κ, Z_e and α into a stochastic soil moisture dynamics model. Here we intentionally refer to rooting depth as the effective, or hydrologically active, rooting depth. Conceptually, this is the average soil water extraction depth, which presumably bears some relationship with actual rooting depth and density as would be measured in the field.

Porporato et al. (2004) combined these three variables into a dimensionless ratio, γ, which is functionally similar to Choudhury's n in that it modifies the partitioning of P between E and R. The ratio is

$$\gamma = \frac{\kappa Z_e}{\alpha}. \tag{3}$$

The variable, κ, replaces Porporato et al.'s (2004) '*s*' and '*n*' variables (where '*s*' was defined as the difference between relative field capacity and wilting point and '*n*' as the fractional soil porosity). Porporato et al. (2004) found that a γ of 5.5 best corresponded to Budyko's curve. With that, and assuming a global-average α of 15 mm and κ of 0.26, those authors calculated average Z_e to be 300–350 mm. Hereafter, we refer to Porporato et al.'s (2004) model simply as the Porporato model.

The general processes understood to cause the observed variability around the Budyko curve can be broadly categorised as: (i) climate variability (i.e., precipitation intensity, seasonality, variance (Donohue et al., 2010b; Gerrits et al., 2009; Koster and Suarez, 1999; Milly, 1994b; Potter and Zhang, 2009); (ii) catchment physical processes (e.g., soil porosity, infiltration rates, catchment slope (Eagleson, 1978; Milly, 1994b; Yang et al., 2006)) and (iii) vegetation functioning (e.g., rainfall interception, perenniality, rooting characteristics, leaf/canopy area, photosynthetic capacity (Donohue et al., 2007; Oudin et al., 2008; Zhang et al., 2001)). Whilst the influence of these processes on plant water use are known to be important, many of them are difficult to quantify both across large areas and through time, and so prove problematic to explicitly parameterise. The utility of the Porporato model is that it effectively encompasses, in varying degrees and in relatively easily implementable ways, the influence of each of these three general processes – α broadly relates to climate variability, κ broadly relates to catchment physical properties and Z_e broadly relates to vegetation water use characteristics. The latter, in particular, is a key variable from a land management perspective. Despite all of this, the stochastic nature of Porporato's model means that it provides only numerical solutions, making an analytical comparison with the Budyko model is difficult.

2.3. Runoff sensitivity

The second aim of this paper is to characterise the sensitivity of runoff to changes in ecohydrologic conditions. Roderick and Farquhar (2011) presented a method for quantifying the sensitivity in R to changes in P, E_p and n using Choudhury's version of the Budyko model (Eq. (2)) and Donohue et al. (2011) applied this spatially across the MDB. Runoff sensitivity was calculated as partial differentials of Eq. (2). Following Roderick and Farquhar (2011), changes in R can be expressed as a function of the three variables of Eq. (2):

$$dR = \frac{\partial R}{\partial P}dP + \frac{\partial R}{\partial E_p}dE_p + \frac{\partial R}{\partial n}dn, \tag{4}$$

where the partial differentials represent the runoff sensitivity coefficients. These three sensitivity coefficients are:

$$\frac{\partial R}{\partial P} = 1 - \frac{E}{P}\left(\frac{E_p^n}{P^n + E_p^n}\right); \tag{5}$$

$$\frac{\partial R}{\partial E_p} = \frac{-E}{E_p}\left(\frac{P^n}{P^n + E_p^n}\right); \tag{6}$$

and

$$\frac{\partial R}{\partial n} = \frac{-E}{n}\left(\frac{\ln(P^n + E_p^n)}{n} - \frac{(P^n \ln P + E_p^n \ln E_p)}{P^n + E_p^n}\right). \tag{7}$$

Later we adapt this framework to the BCP model, quantifying the sensitivity of R to changes in P, E_p, Z_e and α. Additionally, by applying this spatially, we assess the runoff sensitivity to Z_e and α in particular, in key management areas – that is, the high yield zones within the Basin.

2.4. The Murray-Darling Basin

Despite its generally low annual precipitation of approximately 480 mm y^{-1}, the MDB in Australia (Fig. 2A) contributes significantly to Australia's agricultural productivity (Pink, 2008). The Basin's river systems, which underpin much of the Basin's productivity, are fed by the headwater catchments located in the high-rainfall regions along the eastern and south-eastern boundaries. In these regions precipitation seasonality is generally uniform except in the more mountainous (and highest precipitation) areas where it is winter-dominant. These high yield catchments generate two thirds of total basin flows yet constitute only 12% of basin area (Donohue et al., 2011). Donohue et al. (2011) demonstrated that the impact of climatic changes on basin flows will depend largely on the changes occurring in these high yield catchments and argued that long-term planning for these catchments will be critical for managing the hydrological impacts of climate change on the MDB as a whole. Those authors developed four 'high yield zones' within the MDB which provide a spatial framework for analysing the hydrological characteristics of these crucial areas (Fig. 2B). We use these same yield zones here to explore runoff sensitivity.

As one of the key hydrological variables considered here is Z_e, it is pertinent to assess the vegetation characteristics across the five yield zones. Of particular interest is not the absolute effective rooting depth *per se*, but the potential capacity for changes in effective rooting depth. Remotely sensed estimates of fractional green vegetation cover, F (Donohue et al., 2008) – approximately split into the separate contributions from trees, F_t, and grasses, F_g (Donohue et al., 2009) – are shown for the MDB in Fig. 3 and are summarised for the yield zones in Table 1. We expect that trees will generally have greater Z_e than grasses (Schenk and Jackson, 2002).

Each of the four highest yield zones have both reasonably high total vegetation cover and a high proportion of perennial cover, reflecting the relatively wet conditions in these zones compared to the Basin as a whole. The EHYZ encompasses the alpine and the higher sub-alpine regions of the Basin; the low-energy (and low nutrient) conditions of this zone are reflected in lower cover (and productivity) compared to the other high yield zones. The vegetation of this zone is dominated by grassy woodlands and alpine grasslands. The VHYZ has the highest cover and is almost entirely forested. The effective rooting depths of both the EHYZ and the VHYZ are likely to be reasonably static, changing only with major land cover disturbances (e.g., wildfires). By contrast, much of the HYZ that lies outside VHYZ has only a moderate area of tree cover and has a large proportion of agricultural land. Accompanying this land use would be a variety of Z_e which have the potential to be highly temporally dynamic due to land management practices.

In Sections 3 and 4 we describe the development and application of the BCP model, presenting both methods and results in each section. This was done as some of the required input data were themselves modelled – and therefore are results *per se* – even though they remain inputs to the main BCP modelling. Hence, we describe the methods and results of the input data generation in the first part of Section 3, followed by a description of the BCP model itself. In Section 4 we: (i) apply the BCP model to the MDB; (ii) validate modelled MDB R; and (iii) assess the sensitivity of modelled R to changes in the input variables.

3. Development of the Budyko–Choudhury–Porporato model

3.1. Input data

To estimate R with the BCP model (described below), spatially explicit data describing Australian P, E_p, κ, Z_e and α were required over the study period (1981–2006). Whilst grids describing P, E_p

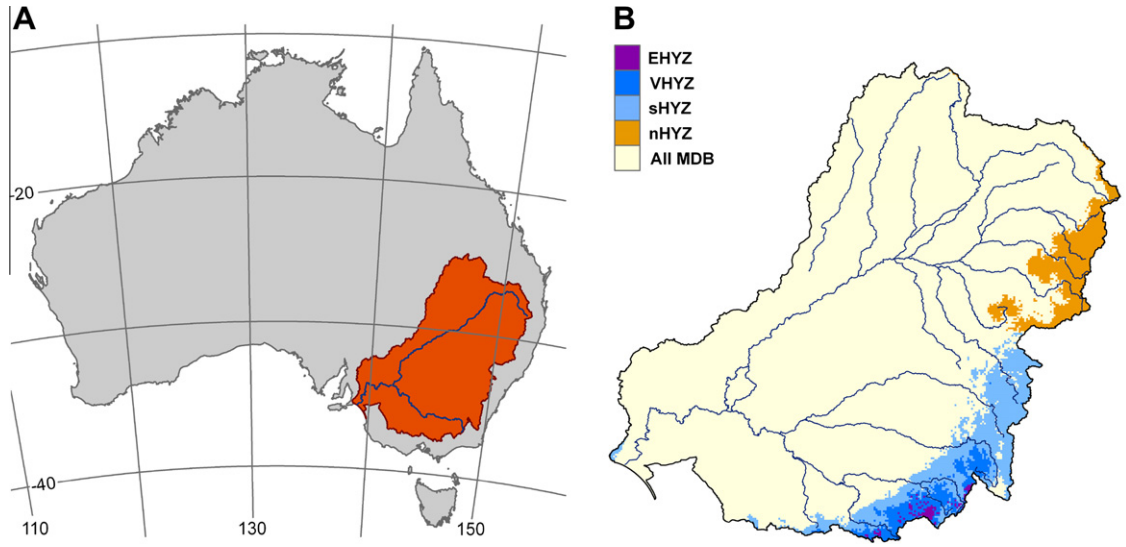

Fig. 2. The Murray-Darling Basin, Australia (A), and the Basin's five yield zones (B). The yield zones are the Extremely High Yield Zone (EHYZ), the Very High Yield Zone (VHYZ), and the southern and northern High Yield Zones (nHYZ and sHYZ). These zones follow Donohue et al. (2011). The fifth yield zone is the whole Basin inclusive of the four high yield zones. In the south, zones are nested such that the VHYZ contains the EHYZ, and the sHYZ contains the VHYZ.

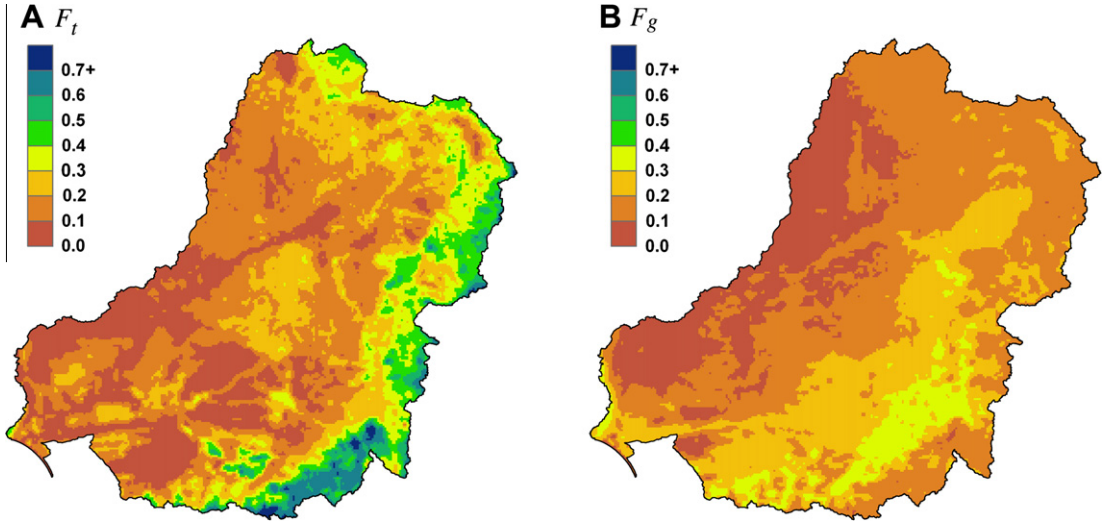

Fig. 3. Fractional vegetation cover across the Murray-Darling Basin averaged over the 1981–2006 period, showing the approximate cover of trees (A) and grasses (B).

Table 1
Zonal average values of the total fractional green vegetation cover approximately split into trees and grasses. Figures in italics represent the percentage of total cover that each functional cover type comprises.

	EHYZ	VHYZ	sHYZ	nHYZ	All MDB
Total cover (F)	0.64	0.74	0.70	0.66	0.38
Tree cover (F_t)	0.52	0.61	0.52	0.50	0.21
	81%	*82%*	*74%*	*76%*	*55%*
Grass cover (F_g)	0.12	0.12	0.18	0.16	0.17
	19%	*18%*	*26%*	*24%*	*45%*

and κ are readily available for Australia, no datasets of Z_e and α of suitable spatial and temporal extent existed prior to this study and had to be specifically developed. All analyses were performed across all of Australia at a 0.05° grid resolution.

3.1.1. Precipitation (P) and potential evaporation (E_p)

Data describing P and E_p came from the daily 0.05° resolution grids of Jones et al. (2009) and Donohue et al. (2010a), respectively. Potential evaporation was derived using Penman's (1948) formulation. The annual average (1981–2006) P and E_p for the MDB are presented in Fig. 4.

3.1.2. Fractional plant-available soil water holding capacity (κ)

An Australia-wide dataset describing κ was generated by normalising the Available Water Holding Capacity (AWHC, mm/m) data from the Atlas of Australian Soils (McKenzie et al., 2000; Northcote et al., 1968). These AWHC data are very coarse both spatially (1:2 million scale) and attribute-wise (highly generalised soil descriptions). The mean Australian κ is 0.093 with a range of 0.021–0.22, and is consistent with the range for Australian soils (0.083–0.223) given by Craze and Hamilton (1991). κ for the MDB is shown in Fig. 5.

3.1.3. Storm depth (α)

No Australia-wide, long-term, sub-daily precipitation data exist from which α could be calculated. However, using long-term Australia-wide grids of rain-day depth (α_d, mm d^{-1}) and site-based

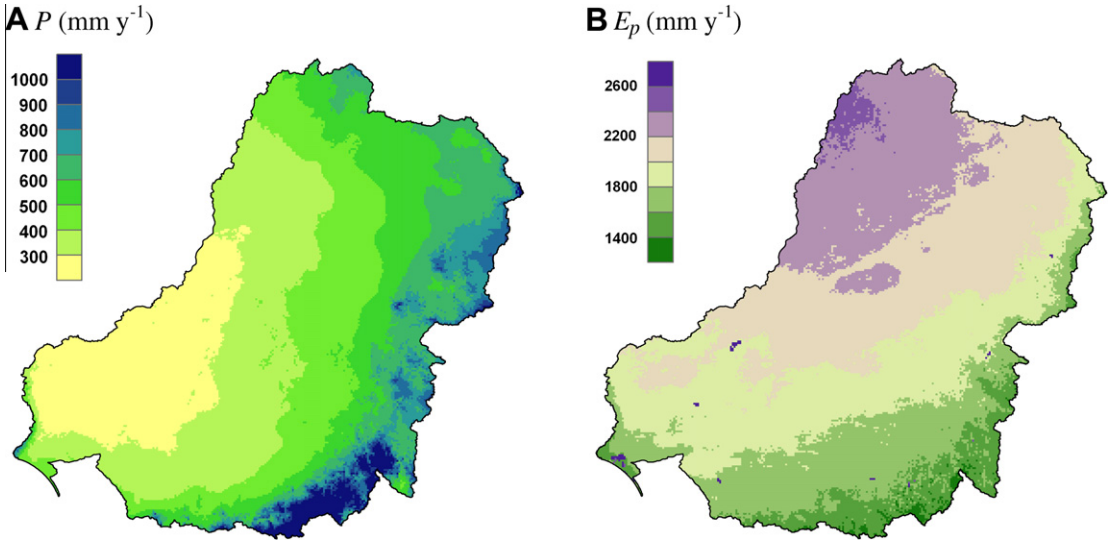

Fig. 4. Long-term average P (A) and E_p (B) for the Murray-Darling Basin, 1981–2006.

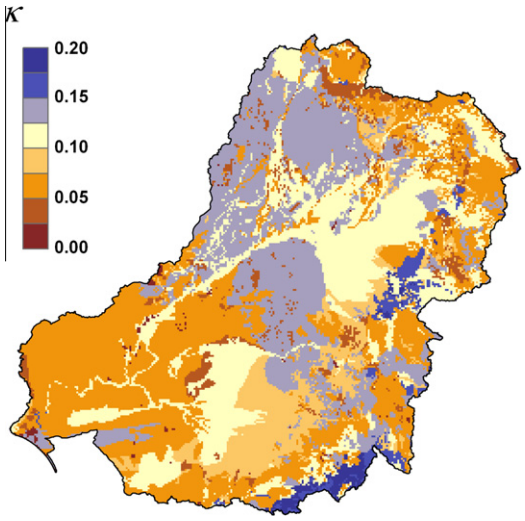

Fig. 5. Fractional plant-available soil water holding capacity (κ) for the Murray-Darling Basin.

pluviograph records, spatial estimates of α were generated by using a α_d to α conversion function. This was performed in three steps. Firstly, Australia-wide grids of α_d were generated from the daily precipitation grids of Jones et al. (2009), being calculated as the mean daily depth of rain days. Average α_d grids were generated for the 1981–2006 period (the period of the main analyses of this paper) and for the 1998–2006 period (the period covered by the pluviograph data).

Secondly, the pluviograph data were analysed to identify average α for each station location. Ten-minute pluviograph data where sourced from the Australian Bureau of Meteorology (L. Renzullo, pers. com.) for 856 sites across Australia. However, these had highly variable temporal coverage (station records varied between 1 and 11 years in length – with gaps – occurring sometime within the 1998–2008 period). We limited analyses to stations that had at least 2500 complete days of data (out of a total 3287 days), which reduced the number of sites to 233 (Fig. 6A). Next a 'storm event' had to be defined. A key characteristic is the minimum inter-storm period (i.e., the period of no precipitation between successive events); how this period is defined depends on the time scale of the processes being investigated (Dunkerley, 2008). We set this to 6 h which we deemed to be the minimum time necessary for the upper soil layers to reach field capacity once saturated; it is also a commonly used value according to Dunkerley (2008). The average depth of all storm events was then determined for each of the 233 stations (Fig. 6A).

The third and last step in generating spatial estimates of α was to derive a conversion function between α_d and α at then to apply this to the Australia-wide α_d grid. The α_d value for each pluviograph location was extracted from the 1998–2006 average α_d grid, and compared with the corresponding pluviograph-derived α (Fig. 6B). This yielded a tight relationship between α_d and α, which was used to convert the 1981–2006 average α_d grid to α. The average α for Australia is 7.0 mm with a range between 2 and 31 mm. Estimated α for the MDB is shown in Fig. 7.

3.1.4. Effective rooting depth (Z_e)

Spatial estimates of Z_e typically need to be modelled. Broad generalisations based on empirical evidence suggest that, under water-limited conditions, the higher the precipitation (or the lower the ϕ) the deeper the rooting depth (Schenk and Jackson, 2002), and the higher the precipitation intensity and/or seasonality under a given P, the deeper roots become in order to maintain the same E (Laio et al., 2002; Milly, 1994a; Porporato et al., 2004; Schenk and Jackson, 2002). Most models of rooting depth (either maximum or effective depth) generally capture the first of these generalisations (Fig. 8A); we are not aware of a model that captures the second. For comparison, Fig. 8B shows the BCP-fitted Z_e for the reference catchments (see below for details). This was estimated using observed P and E_p data, and estimated κ and α, to determine the catchment average Z_e needed to reproduce the observed R according to the BCP model (i.e., by inverting the BCP model).

In Fig. 8A rooting depth peaks at $\phi = 1$ regardless of the model or of whether it is maximum or effective depth, whereas the fitted Z_e peaks between ϕ of 2 and 3. As this same pattern is evident in fitted n (Fig. 10), it seems not to be an artefact of the BCP model itself. Moreover, it has also been observed in the rooting depth data of Schenk and Jackson (2002) for grasslands (Jarvis, 2011). We interpret this pattern as the result of seasonality in the availability of water, as most catchments in this 2–3 ϕ range have either Mediterranean climates or Temperate climates with high summer-time evaporative demand (Peel et al., 2007). If this is the case, then (for these catchments at least) seasonal water supply–demand dynamics are as influential on effective rooting depth – perhaps at times

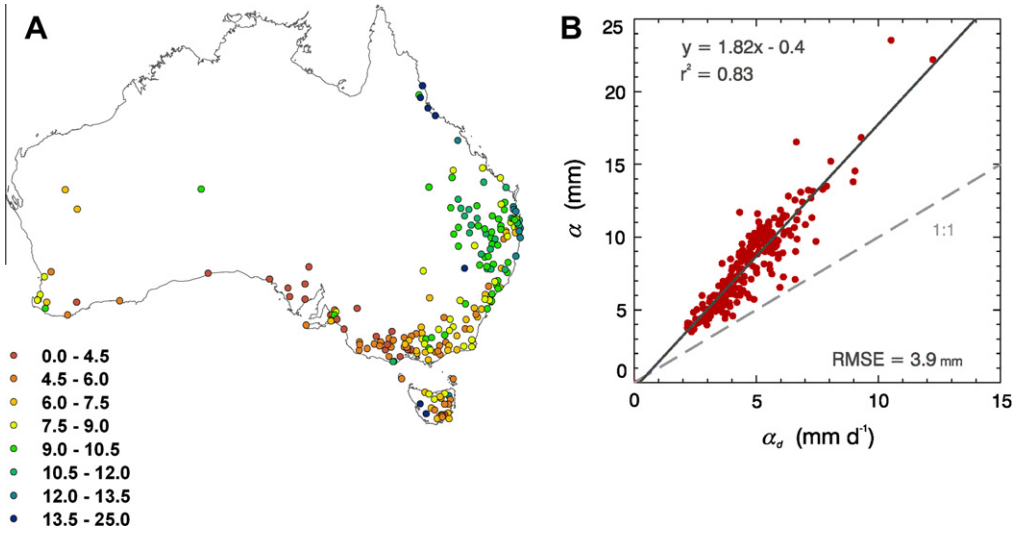

Fig. 6. Mean storm depth derived from 233 pluviograph stations across Australia, compared to grid-derived rain-day depth, for the 1998–2006 period. Plot A shows the distribution of the 233 pluviograph stations and their corresponding α values (in mm). Plot B shows the same α data plotted against grid-derived α_d extracted at the corresponding station locations.

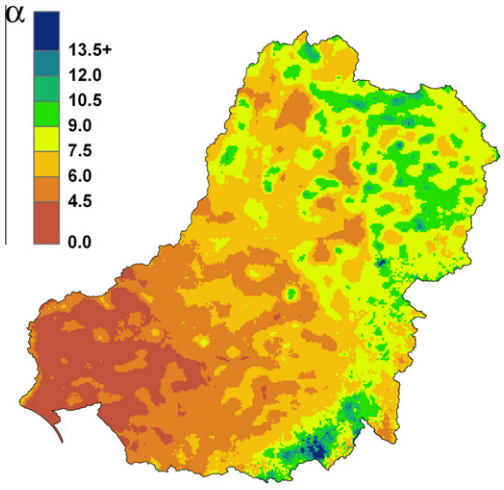

Fig. 7. Estimated storm depth (α) for the Murray-Darling Basin, averaged over the 1981–2006 period.

more influential – as is the total supply of water. Hence, it was imperative that the model used here for estimating Z_e accounted for climate seasonality.

For reference, Fig. 9 provides an indication of the climate seasonality of the study catchments using Köppen climate classes (Stern et al., 2011). Fig. 9A shows the Australian distribution of the Köppen climate classes that contain study catchments, and Fig. 9B shows the Köppen classes plotted as a function of ϕ and fitted Z_e. The humid and sub-arid catchments generally have Temperate climates and, the drier or hotter the summer, the higher the ϕ and the Z_e. Catchments with ϕ above ≈3–4 have Desert and Grassland climates.

Towards this end, we adapted the effective rooting depth model of Guswa (2008). This model estimates Z_e using a carbon cost-benefit approach, identifying the depth at which the trade-off between the cost of adding deeper fine roots is only just balanced by the benefit of the additional carbon assimilated by the extra captured soil water. Guswa (2008) has its genesis in the work of Milly (1993, 2001) and Rodriguez-Iturbe et al. (2001) and so has the same lineage and data requirements as the BCP model. In Guswa (2008) the climate was assumed to be aseasonal and modelling did not consider the effects of water tables or tap roots. Effective rooting depth is determined as a function of the wetness index (W; the reciprocal of ϕ), κ, α and a parameter, A (mm^{-1}), which represents the physiological cost-benefit balance of additional deeper roots. The Guswa (2008) model estimates Z_e of a specified vegetation functional type as

$$Z = \frac{\alpha}{\kappa(1-W)} \ln X. \tag{8}$$

For $W \geqslant 1$, X is calculated as

$$X = W\left(1 + \frac{\kappa}{\alpha}\frac{(1-W)^2}{2A} - \sqrt{\frac{\kappa}{\alpha}\frac{(1-W)^2}{A} + \left(\frac{\kappa}{\alpha}\frac{(1-W)^2}{2A}\right)^2}\right), \tag{9}$$

and, for $W < 1$, X is

$$X = W\left(1 + \frac{\kappa}{\alpha}\frac{(1-W)^2}{2A} + \sqrt{\frac{\kappa}{\alpha}\frac{(1-W)^2}{A} + \left(\frac{\kappa}{\alpha}\frac{(1-W)^2}{2A}\right)^2}\right). \tag{10}$$

The physiological parameter, A (mm^{-1}), for a given vegetation type is:

$$A = \frac{\gamma_r D_r}{L_r W_{ph} T_p f_s}. \tag{11}$$

γ_r is the root respiration rate, D_r is the root-length density, L_r is the specific root length, W_{ph} is the water use efficiency of photosynthesis and f_s is the growing season length (the units of each of these parameters, as well as the values used to parameterise the two vegetation types, are given in Table 2). T_p is the daily potential evaporation rate (mm d^{-1}) for which we used the long-term daily average potential evaporation rate. Effective rooting depth of trees (Z_t, mm) and of grasses (Z_g, mm) is apportioned areally according to the fractional cover of each respective vegetation type, as derived from the separation of the green fractional cover data of Donohue et al. (2009) into the persistent and recurrent cover fractions, respectively. As this model does not explicitly account for bare soil evaporation, this is then normalised by total fractional cover:

$$Z_e = \frac{F_t Z_t + F_g Z_g}{F_t + F_g}. \tag{12}$$

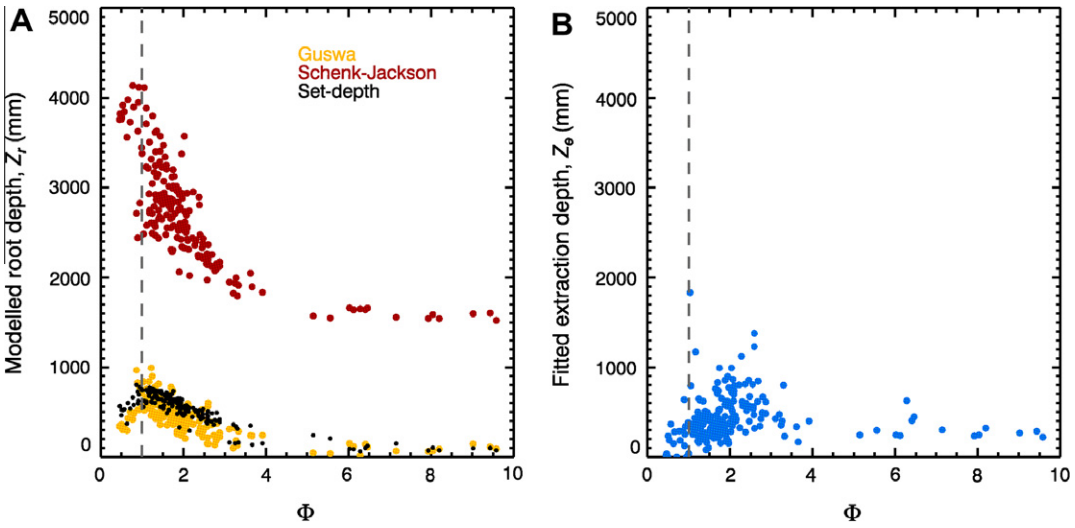

Fig. 8. Comparison of modelled and fitted rooting depth for 193 catchments across Australia. Plot A shows rooting depth estimated using three standard models – Guswa (2008), which estimates effective depth, Schenk and Jackson (2002), which estimates maximum depth, and a set-depth model in which effective tree depth is set to 900 mm, effective grass depth is set to 600 mm and each is apportioned spatially according to long-term, remotely sensed fractional cover values. Plot B shows Z_e fitted to observed catchment hydrological data using the BCP model.

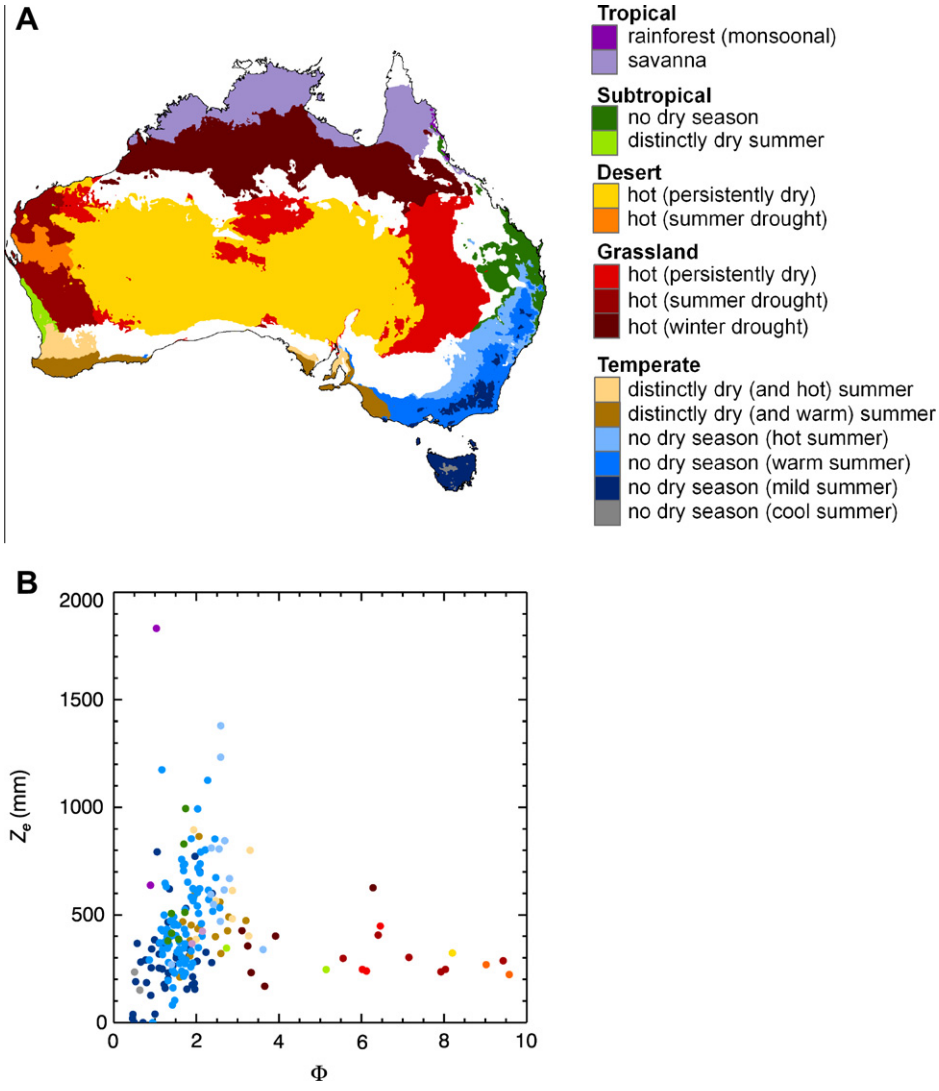

Fig. 9. Köppen climate class compared to fitted rooting depth for the 193 study catchments. Plot A shows the Australian distribution of the Köppen classes that contain the study catchments (that is, white areas represent those climate classes that contain no catchments). In Plot B, the climate classes are plotted as a function of ϕ and Z_e. The colours in Plot B are the same as for Plot A.

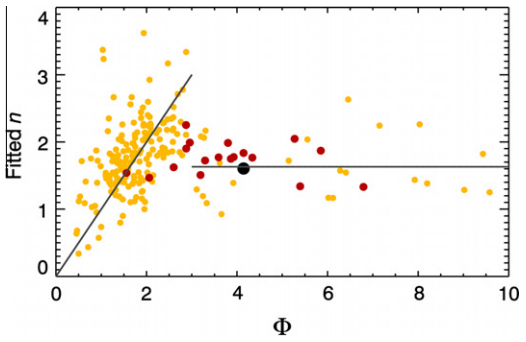

Fig. 10. The relation between fitted n and ϕ for the entire Murray-Darling Basin (black), for the 18 regions (red) and the 193 Australian catchments (orange). A potentially useful heuristic for estimating n (at least for Australian conditions) is $n = \phi$ for $\phi \leqslant 3$, and $n = 1.63$ for $\phi > 3$. The solid lines represent these heuristics. (For interpretation of the references to colour in this figure legend, the reader is referred to the web version of this article.)

Table 2
Parameter values used to calculate effective rooting depth for the two vegetation types. The values are chosen to reflect the general range of values reported elsewhere (Berry and Roderick, 2004; Guswa, 2008; Palese et al., 2000; Reich et al., 2003; Schymanski et al., 2008; Tjoelker et al., 2005).

Variable	Units	Tree	Grass
γ_r	mmol CO_2 g^{-1} d^{-1}	0.5	0.5
D_r	cm cm^{-3}	0.1	0.1
L_r	cm g^{-1}	1500	1500
W_{ph}	mmol CO_2 cm^{-3} H_2O	0.33	0.22
f_s	fraction of year	1.0	0.8

To account for the effects on Z_e of available water seasonality, we adapted the Guswa model to run at a mean monthly time-step so as to represent intra-annual soil water storage dynamics and therefore the intra-annual dynamics in Z_e. From this seasonally varying Z_e time-series an annual average Z_e was derived. Australia-wide, long-term (1981–2006) mean monthly grids of precipitation (P_m, mm mth^{-1}), potential evaporation (E_{pm}, mm mth^{-1}), mean storm depth (α_m, mm) and fractional tree (F_{tm}) and grass (F_{gm}) cover were generated. Five repeating cycles of the monthly average grids were used to give a 60 month time-series so that the model had reached steady-state by the last cycle.

Using a standard bucket model – which is described in Appendix A and shown diagrammatically in Fig. 11 – the mean monthly dynamics in effective rooting depth were calculated in six steps. A seventh step then calculates the annual average Z_e. Here we generally follow the approach taken by Specht (1972).

(1) The current month's ($_{[i]}$) initial soil water store ($S_{1[i]}$, mm) is calculated as the sum of this month's precipitation ($P_{m[i]}$, mm mth^{-1}) and the previous month's stored water, $S_{w[i-1]}$.
(2) The current month's effective rooting depth ($Z_{em[i]}$, mm) is calculated using Eqs. (8)–(12), using the current month's climatic data but replacing $P_{m[i]}$ with $S_{1[i]}$.
(3) Monthly soil water storage capacity ($S_{x[i]}$, mm) is the product of $Z_{em[i]}$ and κ.
(4) The evaporative flux ($E_{m[i]}$, mm mth^{-1}) is calculated using the BCP model (described below), using $Z_{em[i]}$ and again replacing $P_{m[i]}$ with $S_{1[i]}$.
(5) The soil water store after evaporation ($S_{2[i]}$, mm) is the difference between $S_{1[i]}$ and $E_{m[i]}$.
(6) Monthly runoff ($R_{m[i]}$, mm mth^{-1}) is determined conditionally. If the remaining stored soil water is less than this month's storage capacity, runoff ($R_{m[i]}$, mm mth^{-1}) is negligible and stored water at the end of the month ($S_{w[i]}$, mm) equals $S_{2[i]}$. If it is more than the storage capacity, runoff is the difference between stored water and storage capacity, and $S_{w[i]}$ equals the storage capacity.
(7) Having derived a dynamic representation of effective rooting depth (that is, the last 12 months in the 5 year repeated cycle) that incorporates the effects of seasonality in water availability, we identified an effective rooting depth value that represents the annual depth. In doing this we followed the optimality-based allocation principle (Archer et al., 1995; Guswa, 2008; Schenk, 2008; Specht, 1972): in seeking to maximise the capture and storage of water over a year, vegetation in dry places will grow roots just deep enough to buffer the seasonal dynamics in water availability (noting that carbon-balance limitations of deep roots are already accounted for in the Guswa model), whereas where soil

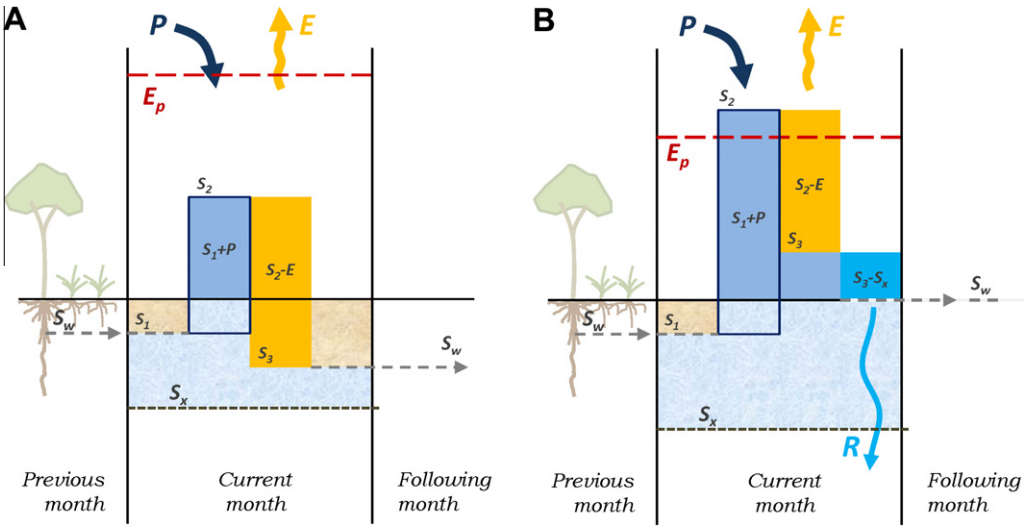

Fig. 11. Schematic representation of the calculation of the monthly soil water storage balance. Plot A represents a month with net drying of soil water and negligible runoff, and plot B represents a month with excess soil water and subsequent runoff.

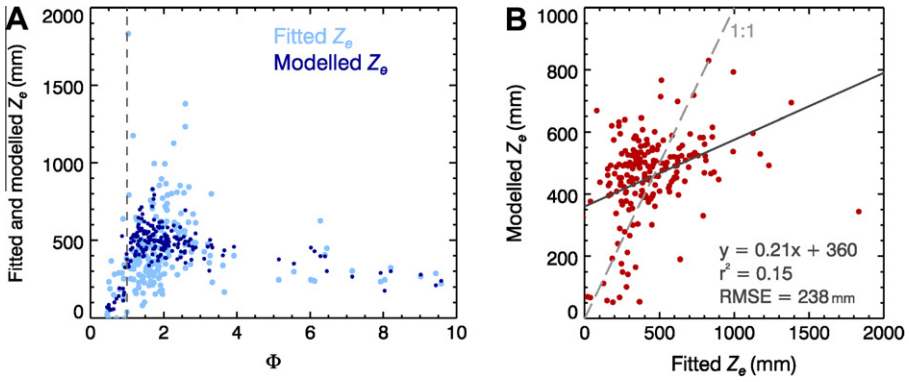

Fig. 12. Comparison of seasonal-Guswa modelled Z_e and fitted Z_e for the 193 Australian catchments. Plot A shows modelled (dark blue) and fitted (light blue) Z_e plotted as a function of ϕ. The dashed line highlights $\phi = 1$. Plot B compares modelled Z_e with fitted Z_e. The solid line represents the line of best fit and the dashed line is the 1:1 line. (For interpretation of the references to colour in this figure legend, the reader is referred to the web version of this article.)

water is in excess, vegetation will grow roots just shallow enough to access enough water to meet the evaporative demand. Hence, for annually water-limited locations, the maximum depth reached during the year was identified as Z_e; and for annually energy-limited locations the minimum depth reached during the year was identified as Z_e.

This model yielded annual Z_e values that show reasonable agreement with fitted Z_e when plotted against ϕ (Fig. 12A) but still struggles to provide a precise representation of fitted Z_e (Fig. 12B). For Australia, modelled Z_e was 313 mm on average and varied between 0 and 1090 mm. Whilst point-based measurements of maximum rooting depth can be substantially greater than these modelled Z_e values (up to tens of metres, Schenk and Jackson, 2002; Stone and Kalisz, 1991), a number of field- and model-based studies of both actual and effective rooting depth suggest that 1000 mm is a reasonable average upper limit for rooting depth (Baker and Ahern, 1989; Jackson et al., 1996; Schenk, 2008; Schenk and Jackson, 2002; Specht, 1972). Z_e across the MDB is shown in Fig. 13. The spatial pattern is dominated firstly by P, and then by κ and α (that is, α of the month with the highest or lowest Z_e, depending on the annual limitation). Of note is that no spatial patterns appear to originate from the tree and grass fractional cover data, indicating that, *as modelled here*, the extent and type of vegetation has a secondary role in determining Z_e compared to climatic and soil conditions.

3.2. The Budyko–Choudhury–Porporato model

To incorporate Porporato's model into the Budyko model, a relationship between Porporato's γ and Choudhury's n was established. Fig. 1 in Porporato et al. (2004) presented numerical solutions for several γ curves in the ϕ–ε dimensional space of the Budyko curve. We obtained, from the authors of that paper, data that show the corresponding ε for every 0.1 increment in ϕ (between 0.1 and 5.0) for six separate γ curves (i.e., 0.5, 1, 2, 5.5, 10 and 20). By numerically solving Eq. (1), we determined the values of n that correspond to the ε values of each of the six γ curves (Fig. 14A). As n varies as a non-linear function of both γ and ϕ, a function for converting between the two parameters over the entire γ domain would be moderately complex. For simplicity, and because γ and n are nearly linearly related for typical values of γ and ϕ, we derived an approximate linear relation between γ and n (Fig. 14B). That is, taking only the five curves for which $\gamma \leqslant 10$, a line was fitted to the n values for which $\phi = 1.0$ (Fig. 14B). We excluded the $\gamma = 20$ curve because it is an extreme value. This gave the approximate linear conversion function:

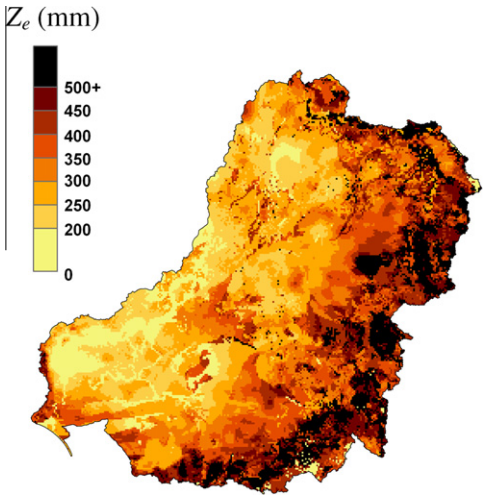

Fig. 13. 1981–2006 Average Z_e for the Murray-Darling Basin modelled using the seasonal Guswa model.

$$n = 0.21\gamma + 0.60, \tag{13}$$

or, in combination with Eq. (3),

$$n = \frac{0.21\kappa Z_e}{\alpha} + 0.60. \tag{14}$$

This relation is shown in Fig. 15. Eqs. (2) and (14) constitute the BCP model.

According to the BCP model, the lower bound of n is approximately 0.6 and, numerically at least, the upper bound appears to be ~4.0. Similar ranges in values have been reported from catchment observations: 1.1–3.1 for 97 catchments in the MDB (Donohue et al., 2011) and 0.6–3.6 for 99 catchments across China (Yang et al., 2009). One circumstance that can lead to n of 0.6 is the absence of vegetation (i.e., $Z_e = 0$ mm) and, conceptually, this provides an estimate of soil evaporation. Using the BCP model and the five input datasets, 1981–2006 average R was modelled for each grid cell across Australia.

4. Application of the Budyko–Choudhury–Porporato model in the Murray-Darling Basin

4.1. Modelled MDB runoff

BCP modelled long-term average n and R for the 1981–2006 period are shown in Fig. 16. The spatial distribution of modelled

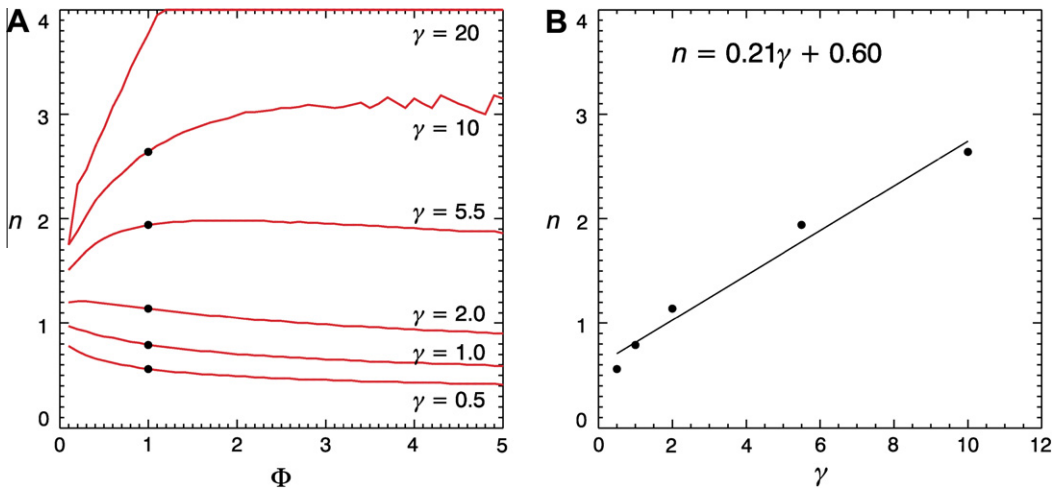

Fig. 14. The relationship between ϕ, n and γ. Plot A shows how n varies with ϕ for each of the six γ curves. The black dots show n for where ϕ = 1.0 and γ = 0.5, 1, 2, 5.5 and 10. Plot B shows the approximate linear relation derived to convert γ to n. The five dots are those from plot A.

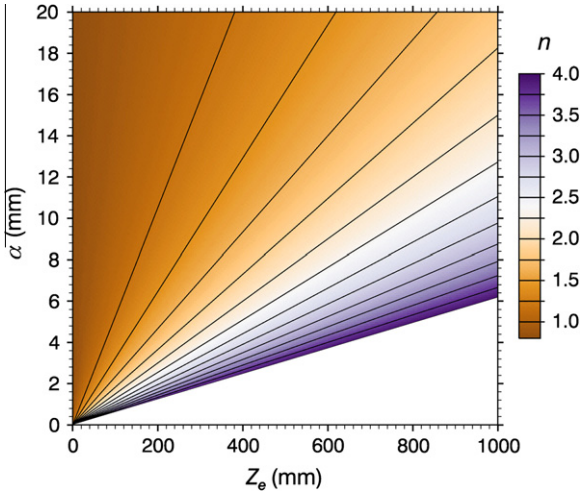

Fig. 15. The relationship between Z_e, α and n. Here κ was held at the Murray-Darling Basin average value of 0.10. In the BCP model, the lowest possible value of n is 0.6. This plot is generated from Eq. (14). Contours are in 0.25 increments.

n shows that high values of n generally occur across the south-eastern half of the MDB (Fig. 16A). The fine scale patterning in n appears to originate partly from κ (Fig. 5) and partly from Z_e (Fig. 13). For individual grids cell across Australia, the range in modelled n is 0.6–4.0, which is the theoretical limit of values, and across the MDB the range is 0.6–3.4. Fig. 16B shows the 1981–2006 modelled R for the Basin. Precipitation overwhelmingly dominates modelled R with high values in the south-east of the Basin, with moderate values in the east generally, and very low R across the west. The influence of n is evident in the spatially fragmented pattern within R.

Summary statistics of the five yield zones of the MDB are provided in Table 3 (the modelled n and R values were calculated from zonally averaged P, E_p, Z_e and α, as opposed to averaging up from grid-cell-based n and R). The zones represent a gradient in climate wetness. κ, α and R all decrease with P whereas Z_e peaks in the nHYZ and n peaks in the VHYZ.

4.2. Validating modelled MDB runoff

Having developed the BCP model and used it to estimate R, we assessed the accuracy of the modelled R against 'reference' flow data at three spatial scales: (i) for the whole MDB; (ii) for 18 sub-basin regions; and (iii) for 193 catchments distributed across Australia. Whole MDB and regional R data are calibrated modelled natural flows (CSIRO, 2008). Reference R data for the 193 catchments are actual observations. The use of these 193 catchments provides an indication of model performance outside the immediate context of the MDB (the range in ϕ across the catchments is 0.45–9.6). The catchment dataset is a subset of the database of unregulated catchment flows compiled by Zhang et al. (2011), selected such that each catchment has at least 20 years of near continuous data and which have experienced little land cover change over the 1981–2006 period. The areas of the regions range between approximately 4000–21,000 km^2 and, for the catchments, between 50 and 100,000 km^2. As some validation data are observations (the catchments) and some are calibrated model outputs, data used for validation will be collectively referred to as reference data throughout this paper. Boundaries of the regions and catchments are shown in Fig. 17.

For the whole Basin, modelled n was 1.58 (Table 4), which is close to the 1.61 obtained by fitting n to reference R (Donohue et al., 2011). The modelled Basin-average R of 29 mm y^{-1} is effectively the same as the reference value.

The comparison of modelled n and R with fitted n and reference R for the sub-basin regions and the Australian catchments are shown in Fig. 18. For the regions, the comparison of BCP-modelled n and n fitted to reference data (Fig. 18A) shows that predictions of n are weak (r^2 of 0). Fig. 18B and C shows that BCP-modelled R was not greatly different from R modelled using the default (i.e., 1.8) value of n. Indeed, both sets of predictions were statistically indistinguishable from the reference data (P-values of 0.44 and 0.33 obtained using the Wilcoxon signed-rank test). However, the accuracy of predictions was higher using the BCP model than the default model (that is, the regression slope of the former was 0.81 compared to 0.74 of the latter – predominantly due to more accuracy predictions for the two wettest regions) and that the precision was lower (r^2 of 0.89 and 0.94, respectively, due to greater scatter in the drier regions). In fact, even better model performance was obtained using the heuristic value of n of 1.63 (see Fig. 10) which yielded $y = 0.85x + 11$ ($r^2 = 0.93$; RMSE = 15 mm y^{-1}). The general aridity of the regions (average ϕ of 3.8) means that estimates of R are not highly sensitive to the accuracy of n.

A similar story emerges for the catchments, except that there is now a slight linear relationship between modelled and fitted n (Fig. 18D). Fig. 18E and F shows that the BCP model was better able

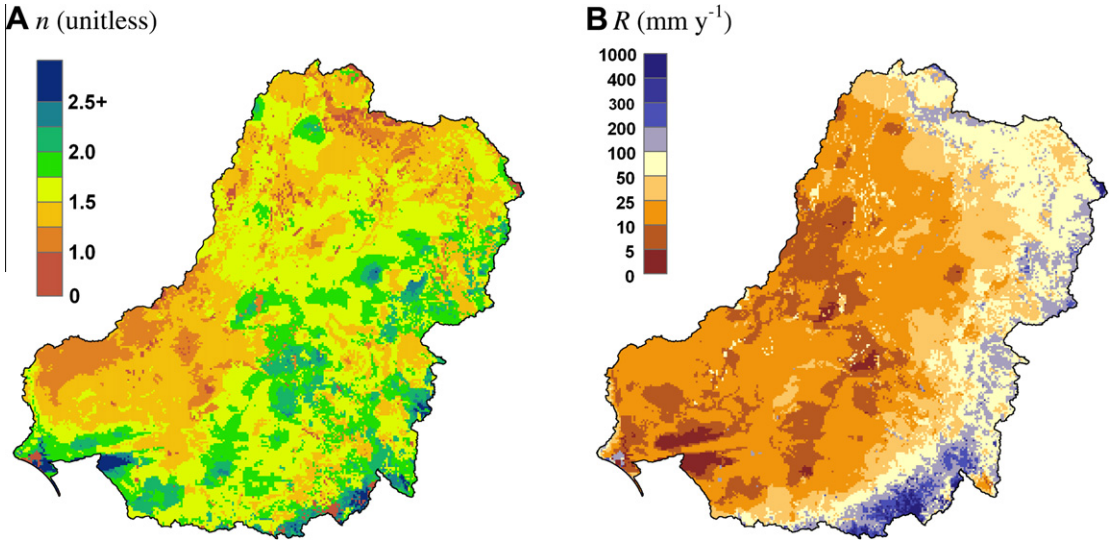

Fig. 16. Long-term average n and R modelled for the Murray-Darling Basin, 1981–2006. Plot A shows modelled n and plot B shows modelled R.

Table 3
Summary statistics of the ecohydrological characteristics of the five Murray-Darling Basin yield zones, 1981–2006. Note that some zones are nested – the VHYZ contains the EHYZ, and the sHYZ contains the VHYZ. Z_e, n and R are modelled values.

	EHYZ	VHYZ	sHYZ	nHYZ	All MDB
P (mm y^{-1})	1487	1191	876	791	476
E_p (mm y^{-1})	1270	1446	1553	1808	1975
κ	0.17	0.15	0.11	0.09	0.10
Z_e (mm)	86	434	480	508	345
α (mm)	13.1	10.7	8.7	8.6	6.8
n	0.83	1.85	1.76	1.68	1.58
R (mm y^{-1})	890	296	139	98	29

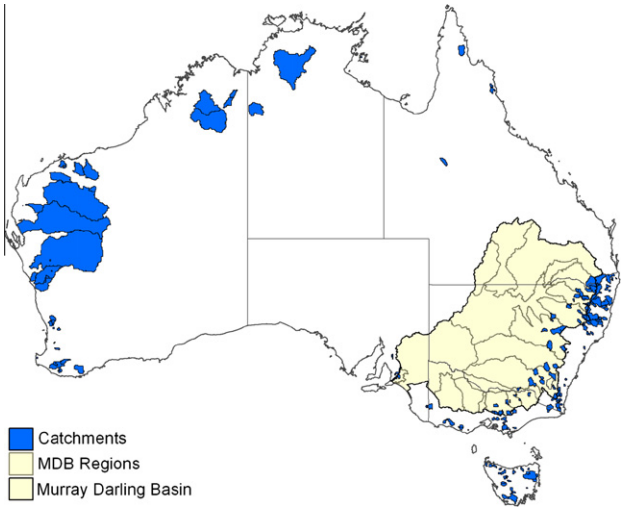

Fig. 17. Distribution of the 18 Murray-Darling Basin regions and the 193 Australian catchments used for model validation.

to predict R than the default model, especially for 'wet' catchments (i.e., $R > \sim 500$ mm y^{-1}) of which there are 20. Whilst both sets of predictions were significantly different from the reference data (both P-values were under 0.01), the slope (0.92) and RMSE (115 mm y^{-1}) from the BCP model demonstrated an increase in accuracy compared to the default model (0.89 and 126 mm y^{-1}, respectively). Again, model precision was slightly lower for the

Table 4
Basin-wide estimates of n and runoff.

Derivation of n	n	R (mm y^{-1})
Fitted	1.61	28
BCP-modelled	1.58	29
Default n	1.80	19
Budyko curve	1.90	16

BCP model. To highlight the improvement in predictions under higher yield conditions, we calculated RMSE values for the wet catchments, which gave 255 mm y^{-1} for the BCP model and 345 mm y^{-1} for the default model. This approximately represents a 10% improvement in model accuracy in these wet catchments relative to their mean flow of 1044 mm y^{-1}.

4.3. Quantifying MDB runoff sensitivity

Using the BCP model, and assuming κ is temporally constant, changes in n can be expressed as

$$dn = \frac{\partial n}{\partial Z_e} dZ_e + \frac{\partial n}{\partial \alpha} d\alpha, \tag{15}$$

and therefore the change in R (Eq. (4)) becomes

$$dR = \frac{\partial R}{\partial P} dP + \frac{\partial R}{\partial E_p} dE_p + \frac{\partial R}{\partial n}\frac{\partial n}{\partial Z_e} dZ_e + \frac{\partial R}{\partial n}\frac{\partial n}{\partial \alpha} d\alpha, \tag{16}$$

where

$$\frac{\partial n}{\partial Z_e} = \frac{0.21\kappa}{\alpha}, \tag{17}$$

and

$$\frac{\partial n}{\partial \alpha} = \frac{-0.21\kappa Z_e}{\alpha^2}. \tag{18}$$

The sensitivity of R to changes in Z_e and in α can each be isolated:

$$\frac{\partial R}{\partial n}\frac{\partial n}{\partial Z_e} = \frac{\partial R}{\partial Z_e} = \frac{-E}{n}\left(\frac{\ln(P^n + E_p^n)}{n} - \frac{\left(P^n \ln P + E_p^n \ln E_p\right)}{P^n + E_p^n}\right)\left(\frac{0.21\kappa}{\alpha}\right), \tag{19}$$

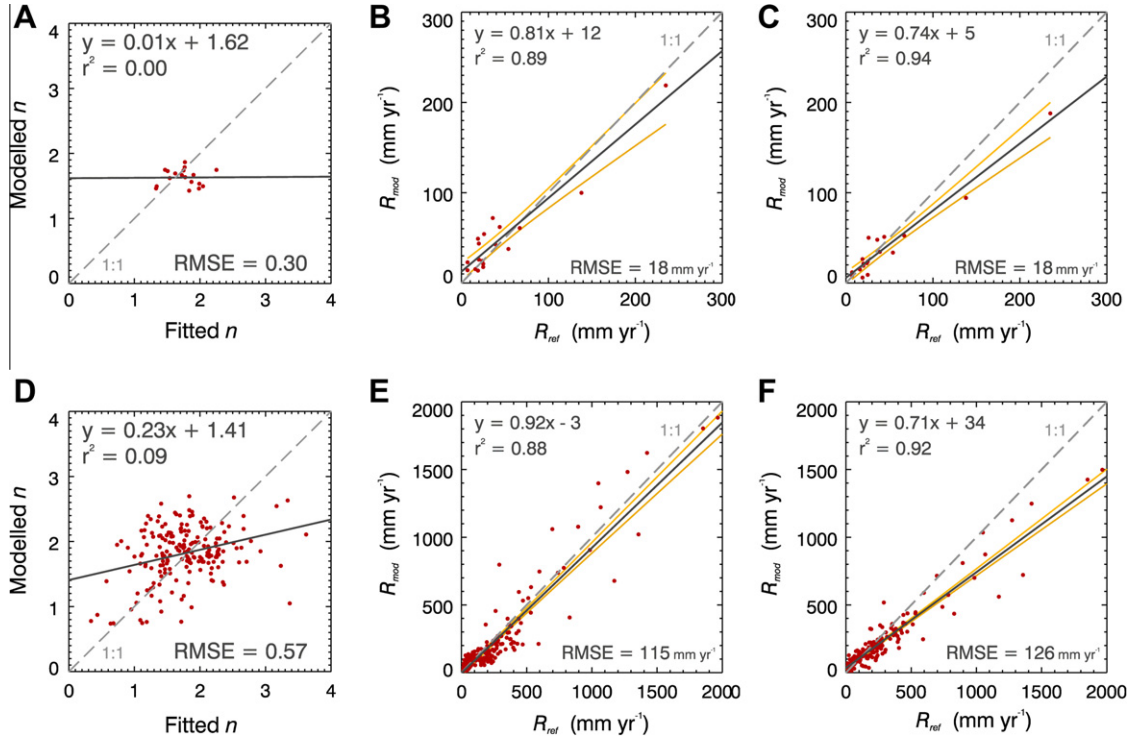

Fig. 18. Comparison of modelled and reference n and R for the Murray-Darling Basin regions and the Australian catchments. Plots A–C represent the 18 sub-basin regions and compare modelled and fitted n (A), modelled and reference R (B). Plot C compares R modelled using $n = 1.8$ with fitted R. Plots D–F are the same as A–C except results are for the 193 catchments. Orange lines show the 95% confidence limits. (For interpretation of the references to colour in this figure legend, the reader is referred to the web version of this article.)

$$\frac{\partial R}{\partial n}\frac{\partial n}{\partial \alpha} = \frac{\partial R}{\partial \alpha} = \frac{-E}{n}\left(\frac{\ln(P^n + E_p^n)}{n} - \frac{(P^n \ln P + E_p^n \ln E_p)}{P^n + E_p^n}\right)\left(\frac{-0.21\kappa Z_e}{\alpha^2}\right). \quad (20)$$

The sensitivities of R to changes in the four ecohydrological variables (that is, P, E_p, Z_e and α) were calculated for each grid cell using Eqs. (5), (6), (19), and (20). These sensitivities are summarised for the five MDB yield zones in Table 5 and displayed spatially in Fig. 19. Each of the sensitivities are related to climate dryness in that, as P decreases, R generally becomes less sensitive to changes in each variable. Runoff in the EHYZ is highly sensitive to changes in Z_e, with results indicating that R would decrease by about 10 mm y^{-1} for every 10 mm increase in Z_e (that is, $\partial R/\partial Z_e$ is -1.0 mm y^{-1}/mm). By contrast, $\partial R/\partial Z_e$ is much lower in the other yield zones, altering R by approximately 2–5 mm y^{-1} for the same change in Z_e. The values of $\partial R/\partial \alpha$ are relatively large because the actual values of α are small – that is, a 1 mm change in α constitutes a reasonably large proportion of average α (between 7% and 15%, see Table 3) whereas a 1 mm change represents a very small proportion of any of the other three variables.

The sensitivity coefficients in Table 5 show the sensitivities in R to changes in the four variables. From the sensitivities alone it is difficult to discern the relative importance of each variable. To give an indication of this, the 'typical variability' observed in each variable between 1981 and 2006 was determined (represented using the standard deviation in annual values, Table 5). In conjunction with the modelled sensitivity coefficients, the typical variability of each input variable was used to determine its contribution to the typical variability in R (Table 5). For example, for the EHYZ, the sensitivity of R to P (i.e., $\partial R/\partial P$) is 0.81 mm y^{-1}/mm y^{-1} and the typical variability in P (i.e., dP) is 366 mm y^{-1}. The product of these two figures yields an estimate of the typical variability in R caused by that in P ($\partial R/\partial P\ dP$), which is 296 mm y^{-1}. In terms of the climatic drivers, Table 5 shows that year-to-year variations in P cause the greatest variability in R, generally followed by variability in α and then E_p. Note, however, that α and Z_e increase in relative importance compared to R as climatic dryness increases.

Table 5
Zonal summaries of runoff sensitivities to changes in ecohydrological conditions for the 1981–2006 period. Shown for each variable and zone is the runoff sensitivity coefficient (e.g., $\partial R/\partial P$), the observed variability in that variable (e.g., dP), and the typical variability in runoff caused by the driving variable (e.g., $\partial R/\partial P\ dP$). The latter value is determined as the product of the two former values and assumes an *increase* in the driving variable (the effect of a *decrease* in the driving variable is found by changing the sign of the product). dZ_e is the difference between tree and grass Z_e modelled for each zone.

	Units	EHYZ	VHYZ	sHYZ	nHYZ	MDB
$\frac{\partial R}{\partial P}$	mm y^{-1}/mm y^{-1}	0.81	0.55	0.39	0.31	0.17
dP	mm y^{-1}	366	297	224	174	141
$\frac{\partial R}{\partial P}dP$	mm y^{-1}	296	163	87	54	24
$\frac{\partial R}{\partial E_p}$	mm y^{-1}/mm y^{-1}	−0.25	−0.23	−0.13	−0.08	−0.03
dE_p	mm y^{-1}	69	69	78	74	86
$\frac{\partial R}{\partial E_p}dE_p$	mm y^{-1}	−17	−16	−10	−6	−3
$\frac{\partial R}{\partial Z_e}$	mm y^{-1}/mm	−1.00	−0.50	−0.32	−0.25	−0.16
dZ_e	mm	9	133	160	158	104
$\frac{\partial R}{\partial Z_e}dZ_e$	mm y^{-1}	−9	−67	−51	−40	−17
$\frac{\partial R}{\partial \alpha}$	mm y^{-1}/mm	10.88	18.71	16.76	14.38	7.96
$d\alpha$	mm	2.0	1.6	1.4	1.4	1.5
$\frac{\partial R}{\partial \alpha}d\alpha$	mm y^{-1}	22	30	23	20	12

Against this assessment of typical variability is the affect on R of landscape-wide changes in vegetation cover. A conversion from forest to grassland, or vice versa, has the potential to cause greater changes in R than the typical variability in either α or E_p. One point

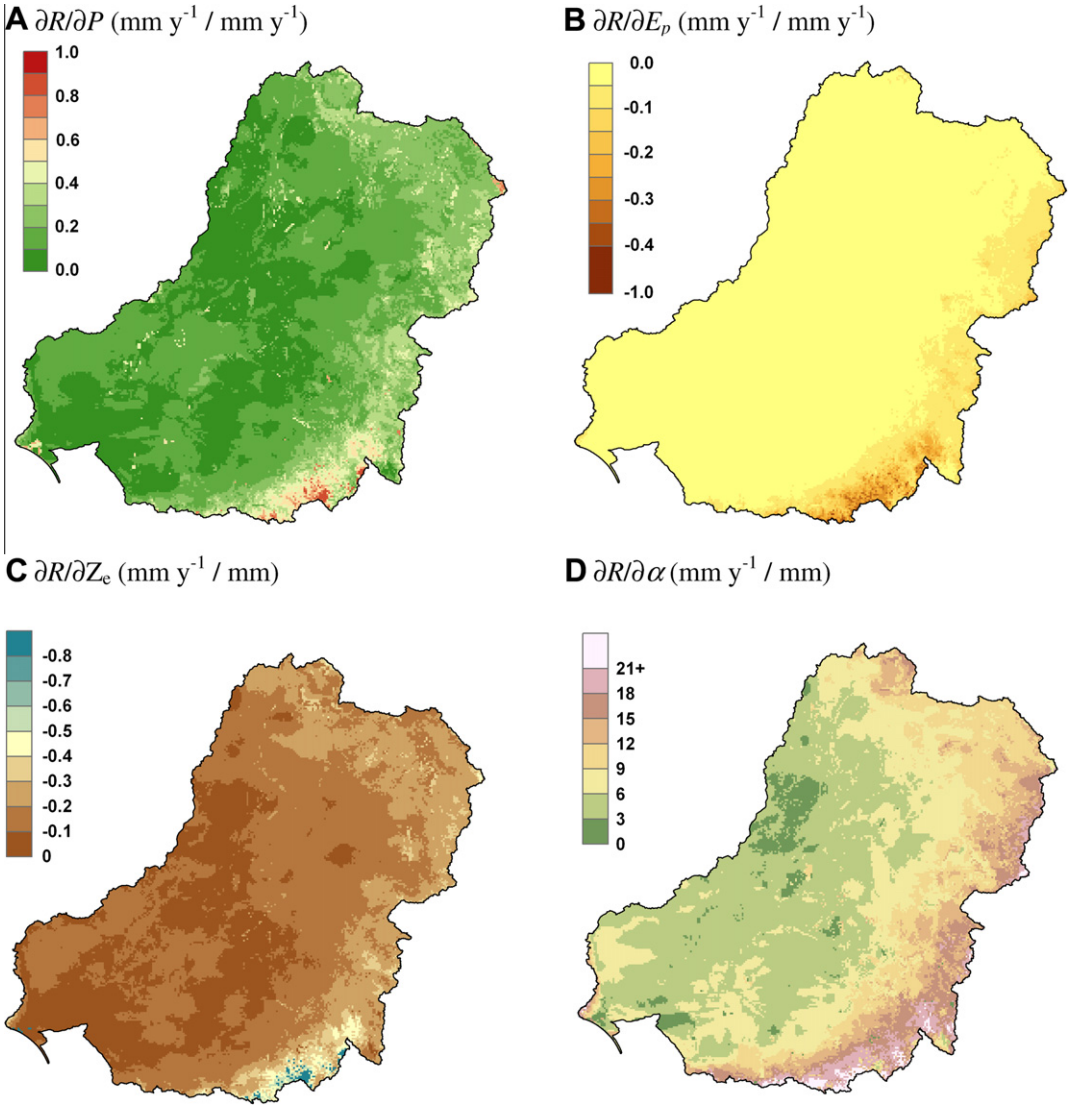

Fig. 19. The sensitivity of R to changes in the four ecohydrological variables across the Murray-Darling Basin, 1981–2006. Plots A–D show the sensitivity of R to changes in P, in E_p, in Z_e and in α, respectively.

that is well demonstrated here is that the overall impact on R of changes in Z_e is a function of *both* runoff sensitivity and the difference between Z_t and Z_g. For example, even though $\partial R/\partial Z_e$ is extremely high in the EHYZ, the estimated difference between Z_t and Z_g is so small (9 mm – this zone supports only alpine and sub-alpine vegetation) that the overall impact of land cover conversion in this zone is negligible. By contrast, despite lower $\partial R/\partial Z_e$ values in the VHYZ and the two HYZs, the greater differences between tree and grass Z_e in these zones are expected to produce a far greater change in R.

Overall, this sensitivity analysis suggests that a given future change in P will have the greatest impact on R in the highest yield zones, and that land-cover-induced changes in Z_e are likely to cause similar or greater changes in R than future changes in either E_p or α, at least whilst changes remain close to the bounds of typical variability as defined here.

5. Discussion

The BCP model was shown to improve R predictions under high yield conditions compared to the default value of n. However, there remains considerable scatter in BCP predictions, indicating that there are localised variations in catchment behaviour that are not being captured in the BCP modelling. This is most likely a reflection of the scale limitations of the input data used to model n. Whilst the dataset used to estimate κ has very low spatial and attribute resolutions, it represents the only soils dataset that is spatially consistent across all of Australia. Additionally, long-term α is expected to contain fine-resolution spatial variation in high-relief landscapes – which are often also the high water yielding landscapes. It is difficult to verify this expectation as no long-term, spatially extensive data describing Australian α exist. Here we used point-based pluviograph-derived values of α to approximately convert spatial estimates of rain-day depth to α. Whilst this approach was necessary, it will have inevitably introduced some error into the modelling. Overall model accuracy is expected to improve as finer scale and higher quality κ and α data become available.

Observations of Z_e are scarce and so validating Z_e across large areas is difficult. Even if rooting depth observations were spatially extensive, there is a conceptual disconnect between what can be measured in the field (usually maximum depth) and 'effective' hydrological depth (or, more correctly, average extraction depth). Added to this is that Z_e, as estimated here, is an area average

whereas observations are typically point-based (and taken directly under individual plants!). Currently, the most practical approach to validating Z_e is to fit Z_e to R observations by inverting a hydrological model and compare modelled Z_e to fitted Z_e.

An important step in developing the BCP model was the development of a model of effective rooting depth that incorporates the effects of climate seasonality. It became apparent that seasonality in the water supply–demand dynamics greatly influences effective rooting depth, to the point that, in semi-arid climates, seasonality can be just as influential on Z_e as the total water supply. As the study catchments that displayed this behaviour had almost exclusively Temperate climates, the above generalisation is restricted to this climate type. We do not expect it hold under Tropical climates, where the maximum Z_e may well occur when ϕ is around 1 (the highest fitted Z_e in this study [1832 mm] was from a Tropical catchment [ϕ = 1.03]), nor under arid climates where the effects of the overall paucity of water outweighs any effects of seasonality.

A previously noted phenomenon in water-limited environments is that, for a given ϕ or P, a greater proportion of plant resources will be allocated below-ground under a seasonal climate resulting in relatively less above-ground biomass (Field et al., 1992; Schenk and Jackson, 2002). One implication of this finding is that the relationship between vegetation cover and Z_e does not vary linearly with annual average ϕ or P. For example, a sparsely forested catchment under a highly seasonal climate may have a greater Z_e than a more heavily forested catchment under an aseasonal climate – regardless of whether that latter catchment is in a higher rainfall zone. The failure of the set-depth effective rooting model (Fig. 8A), which apportioned fixed root depths according to tree and grass cover, demonstrated the inadequacy of this assumption.

At the regional scale, the BCP model predicted n with low precision but predicted R with at least as much accuracy as predictions made with a default value of n. Most of these regions were arid or semi-arid and under such conditions R is not sensitive to small variations in n. This begs the question: under what conditions is the precision of n important? A simple generalisation can be made based on Eq. (7) – the smaller n is, or the closer to 1 that ϕ is, the more sensitive R is to variations in n. Conversely, for arid conditions (i.e., $\phi > 3$) R is relatively insensitive to n for values of n above approximately 1.5. For semi-arid conditions (i.e., $2 < \phi < 3$), R is relatively insensitive to n only when n is above 2.0–2.5.

The Zhang model (Zhang et al., 2001) has received widespread use as a tool for estimating the effect of changes in forest cover on long-term stream flow. Its value lies in its simplicity and practical utility. The BCP model builds on the Zhang model in that it maintains model simplicity and transparency and, in fact, can reproduce the Zhang curves. However, the BCP model moves away from the qualitative (that is, the forest/non-forest classification of vegetation) and empirical nature of the Zhang model. Instead the BCP model quantitatively incorporates three process-based ecohydrological variables that relate to soils, climate variability and vegetation functioning. Indeed, the disconnect between forest extent and rooting depth (described above) is probably a key reason why the Zhang model has not performed well under all climatic conditions (Donohue et al., 2010b; Oudin et al., 2008).

Whilst rooting depth was modelled in a semi-dynamic manner – that is, intra-annual water storage changes were quantified – the BCP model as applied here is restricted to steady-state conditions, where the changes in stored water are assumed negligible compared to the total flux of water over the period of interest. Consequently, the model has temporal scale dependencies and should be used with care under non-stationary conditions. If, on the other hand, changes in storage can be quantified, this model can be freely used under transient conditions.

Since Z_e is the only vegetation-related variable in the BCP model (and since vegetation is a key medium through which R can be manipulated by management), the incorporation of Z_e into Budyko's model has many practical implications. For example, the insight that the average hydrological effects of vegetation cover changes depend not only on runoff sensitivity but also on how much Z_e can vary leads to some important (and quantifiable) implications. In the context of the MDB, the highest water yielding catchments are, on the whole, forested and are reserved for conservation or timber production purposes. It is reasonable to assume that the management of these catchments will continue unchanged and hence Z_e will remain reasonably constant over the long-term (assuming no changes in fire or management regimes occur). On the other hand, in the moderate water yielding catchments – which are largely under agriculture – land management has the greatest capacity to change Z_e and therefore to influence R. Based on the modelled values of tree and grass Z_e and subsequent BCP-modelled R, the whole-scale conversion of grasslands to forest in a moderate water yielding catchments (i.e., in the nHYZ) would likely produce an increase in Z_e from around 390 mm to 550 mm and an associated decrease in R from 130 to 80 mm y^{-1}. A similar land cover conversion in the sHYZ (in this case, a change in Z_e from ~390 mm to 550 mm) could decrease R from approximately 170 to 110 mm y^{-1}. For comparison, the clearing of a forested catchment in the VHYZ (i.e., a 130 mm *decrease* in Z_e) could *increase* R from 280 to 360 mm y^{-1}.

The possible direct effects of climate change on Z_e are not well understood. Assuming that the CO_2 fertilisation effect will enhance vegetation growth in water-limited environments (Farquhar, 1997; Field et al., 1995) and that it will benefit woody (deep rooted) species more that non-woody species (Berry and Roderick, 2006; Field et al., 1992; Polley, 1997), then a reasonable expectation is that the abundance of woody vegetation may increase as atmospheric CO_2 concentrations increase. Indeed an increase in perennial vegetation cover has been observed over the past few decades across much of Australia (Donohue et al., 2009). If this is a general and ongoing phenomenon, then an overall increase in Z_e should occur (e.g., Iversen, 2010) and, according to the BCP model, a decrease in runoff in such water-limited environments (all else being equal). Even though the response of roots to climate change is uncertain, the incorporation of Z_e into the Budyko framework provides a means for quantitatively examining the role of effective rooting depth dynamics (and through it the different water use characteristics of broad vegetation functional types) under any future climate/land use scenario.

As α is one of two variables that describe precipitation intensity (the other being rain frequency), the incorporation of α into the Budyko model provides a means of assessing the sensitivity of runoff to changes in precipitation intensity. According to these analyses, MDB runoff becomes less sensitive to changes in α as overall dryness increases, but in relative terms (i.e., compared to total flows) runoff sensitivity to α increases as dryness increases (Table 5). In addition, the sensitivity of runoff to changes in Z_e is moderated by α – the higher the storm depth, the lower the sensitivity, all else being equal. Precipitation intensity has been predicted to increase as the atmospheric temperature increases (Huntington, 2006; Trenberth et al., 2007). Accordingly (but depending on how rain frequency changes) it is feasible that α may increase with time, which will produce an overall increase in runoff, all else being equal. As an example, for all the high yielding catchments in the MDB, a 10% or 20% increase in α would increase R from 98 mm y^{-1} to 110 mm y^{-1} and 123 mm y^{-1}, respectively.

Whilst fractional plant-available water holding capacity varies considerably across space, it has been assumed to be temporally static and does not feature in the runoff sensitivity analysis. κ is an important component of the BCP model, and of Porporato's original model. For one, it is an influential variable within the model. This is clear from the spatial patterns occurring in the model

outputs. Also, κ *can* change over time due to, for example, mechanical compaction or the effects of intense fires. Despite κ being reasonably static, it is an important variable within the BCP model.

6. Conclusion

In order to incorporate the effects of soil water holding capacity, effective rooting depth and storm depth into Budyko's (1974) hydrological model, and then assess the hydrological effects changes in the latter two variables in particular, we combined the ecohydrological model of Porporato et al. (2004) with Budyko's model. This 'Budyko–Choudhury–Porporato', or BCP, model provides a method to *a priori* estimate *n*. Here we employed a carbon-balance-based model of effective rooting depth that differentiates between trees and grasses and, significantly, accounts for the effects of climate seasonality on depths. After testing the BCP model across the Murray-Darling Basin in Australia, we applied the runoff sensitivity framework of Roderick and Farquhar (2011) to assess the effects on runoff of changes in effective rooting depth and storm depth in the strategically important high yield zones within the Basin.

Basin-wide, 1981–2006 average runoff was accurately predicted, being within 1 mm y^{-1} of a previously modelled natural flow of 28 mm y^{-1}. The overall accuracy of predictions at the finer spatial scales of the 18 sub-basin regions and of the 193 catchments was also high but with considerable scatter, reflecting the high spatial variability inherent in catchment behaviour. Importantly, estimates from the 20 highest water yielding catchments (>~500 mm y^{-1}) were considerably more accurate when made with the BCP model than when made using a default value of *n* (i.e., $n = 1.8$).

The high yield zones of the Basin make up a small fraction of the Basin's area, yet management of catchments within these zones is critical to the management of overall Basin flows. These are therefore key areas to focus activities aimed at mitigating potential impacts of climatic changes. Analysis of runoff sensitivity shows that changes in precipitation have by far the greatest impact on runoff in the high yield zones, followed generally by changes in effective rooting depth and then storm depth. By contrast, across the Basin as a whole – which is reasonably arid – the influences of changes in effective rooting depth and storm depth become almost as important as changes in precipitation.

The novelty of the BCP model is that it quantitatively incorporates the effects of soil water holding capacity, effective rooting depth and storm depth whilst maintaining the simplicity and transparency of the original Budyko model. The BCP model has potential applications in the natural resource management and policy development arena, as it incorporates a key ecohydrological effect of vegetation, which is itself the prime medium through which catchment yields can be directly manipulated and managed. Perhaps counter-intuitively, it may not be the areas where runoff is highest (or where runoff sensitivity is highest) where management efforts may have the greatest potential to change runoff. Instead, the greatest impact might be had in those areas with only moderate runoff (and runoff sensitivity) but where the climatic conditions and existing land uses allow for the greatest changes in effective rooting depth to be implemented.

Acknowledgments

We are grateful to Linda Gregory, John Gallant and David Jacquier, of CSIRO Land and Water, for providing the Atlas of Australian Soils data; to Amilcare Porporato and Xue Feng, of Duke University, for providing data describing the γ function; and to Luigi Renzullo, of CSIRO Land and Water, for providing the 10-min pluviograph data (made available through the Water Information Research and Development Alliance [WIRADA] between CSIRO and the Bureau of Meteorology). R.J.D. and T.R.M. acknowledge the support of CSIRO's *Water for a Healthy Country* and *Sustainable Agriculture* Flagships, the Murray-Darling Basin Authority (Jason Alexandra) and of WIRADA. M.L.R. acknowledges the support of the Australian Research Council (DP110105376).

Appendix A

See Table A1.

Table A1
Equations describing the calculation of mean monthly and annual average effective rooting depths.

Step	Equation		
1		$S_{1[i]} = P_{m[i]} + S_{w[i-1]}$	(21)
2		$Z_{em[i]} = f(S_{1[i]}, E_{pm[i]}, \alpha_{m[i]}, \kappa)$	(22)
3		$Sx[i] = \kappa Z_{em}[i]$	(23)
4		$E_{m_{[i]}} = f(S_{1[i]}, E_{pm[i]}, \kappa, \alpha_{m[i]}, Z_{r[i]})$	(24)
5		$S_{2[i]} = S_{1[i]} - E_{m[i]}$	(25)
6	For $S_{2[i]} \leqslant S_{x[i]}$,	$R_{m[i]} = 0$	(26)
		$S_{w[i]} = S_{2[i]}$	(27)
	For $S_{2[i]} < S_{x[i]}$,	$R_{m[i]} = S_{2[i]} - S_{x[i]}$	(28)
		$S_{w[i]} = S_{x[i]}$	(29)
7	For $\phi \leqslant 1.0$	$Z_e = \min(Z_{m[49-60]})$	(30)
	For $\phi > 1.0$	$Z_e = \max(Z_{m[49-60]})$	(31)

References

Archer, S., Schimel, D.S., Holland, E.A., 1995. Mechanisms of shrubland expansion – land-use, climate or CO_2. Clim. Change 29 (1), 91–99.
Baker, D.E., Ahern, C.R., 1989. Estimates of effective rooting depth for predicting available water capacity of Burdekin soils, Queensland. Aust. J. Soil Res. 27, 439–454.
Berry, S.L., Roderick, M.L., 2004. Gross primary productivity and transpiration flux of the Australian vegetation from 1788 to 1988 AD: effects of CO_2 and land use change. Global Change Biol. 10 (11), 1884–1898.
Berry, S.L., Roderick, M.L., 2006. Changing Australian vegetation from 1788 to 1988: effects of CO_2 and land-use change. Aust. J. Bot. 54 (4), 325–338.
Budyko, M.I., 1974. Climate and Life. International Geophysics Series, vol. 18. Academic, New York, 508 pp.
Calder, I.R., 1993. Hydrologic effects of land-use change. In: Maidment, D.R. (Ed.), Handbook of Hydrology. McGraw Hill, Sydney.
Choudhury, B.J., 1999. Evaluation of an empirical equation for annual evaporation using field observations and results from a biophysical model. J. Hydrol. 216 (1/2), 99–110.
Craze, B., Hamilton, G.J., 1991. Soil physical properties. In: Charman, P.E.V., Murphy, B.W. (Eds.), Soils – Their Properties and Management. Sydney University Press, South Melbourne, pp. 147–164.
CSIRO, 2008. Water Availability in the Murray-Darling Basin. A Report to the Australian Government from the CSIRO Murray-Darling Basin Sustainable Yields Project. CSIRO, Canberra, 67 pp.
Donohue, R.J., Roderick, M.L., McVicar, T.R., 2007. On the importance of including vegetation dynamics in Budyko's hydrological model. Hydrol. Earth Syst. Sci. 11, 983–995.
Donohue, R.J., Roderick, M.L., McVicar, T.R., 2008. Deriving consistent long-term vegetation information from AVHRR reflectance data using a cover-triangle-based framework. Remote Sens. Environ. 112 (6), 2938–2949. http://dx.doi.org/10.1016/j.rse.2008.02.008.
Donohue, R.J., McVicar, T.R., Roderick, M.L., 2009. Climate-related trends in Australian vegetation cover as inferred from satellite observations, 1981–2006. Global Change Biol. 15 (4), 1025–1039. http://dx.doi.org/10.1111/j.1365-2486.2008.01746.x.
Donohue, R.J., McVicar, T.R., Roderick, M.L., 2010a. Assessing the ability of potential evaporation formulations to capture the dynamics in evaporative demand within a changing climate. J. Hydrol. 386, 186–197. http://dx.doi.org/10.1016/j.jhydrol.2010.03.020.
Donohue, R.J., Roderick, M.L., McVicar, T.R., 2010b. Can dynamic vegetation information improve the accuracy of Budyko's hydrological model? J. Hydrol. 390, 23–34. http://dx.doi.org/10.1016/j.jhydrol.2010.06.025.
Donohue, R.J., Roderick, M.L., McVicar, T.R., 2011. Assessing the differences in sensitivities of runoff to changes in climatic conditions across a large basin. J. Hydrol. 406, 234–244. http://dx.doi.org/10.1016/j.jhydrol.2011.07.003.
Dunkerley, D., 2008. Identifying individual rain events from pluviograph records: a review with analysis of data from an Australian dryland site. Hydrol. Process. 22 (26), 5024–5036.
Eagleson, P.S., 1978. Climate, soil, and vegetation 1. Introduction to water-balance dynamics. Water Resour. Res. 14 (5), 705–712.

Farquhar, G.D., 1997. Carbon dioxide and vegetation. Science 278 (5342), 1411.
Field, C.B., Chapin, F.S., Matson, P.A., Mooney, H.A., 1992. Responses of terrestrial ecosystems to the changing atmosphere – a resource-based approach. Annu. Rev. Ecol. Syst. 23, 201–235.
Field, C.B., Jackson, R.B., Mooney, H.A., 1995. Stomatal responses to increased CO_2 – implications from the plant to the global-scale. Plant Cell Environ. 18 (10), 1214–1225.
Gerrits, A.M.J., Savenije, H.H.G., Veling, E.J.M., Pfister, L., 2009. Analytical derivation of the Budyko curve based on rainfall characteristics and a simple evaporation model. Water Resour. Res. 45. http://dx.doi.org/10.1029/2008WR007308.
Guswa, A.J., 2008. The influence of climate on root depth: a carbon cost-benefit analysis. Water Resour. Res. 44 (2). http://dx.doi.org/10.1029/2007WR006384.
Huntington, T.G., 2006. Evidence for intensification of the global water cycle: review and synthesis. J. Hydrol. 319 (1–4), 83–95. http://dx.doi.org/10.1016/j.jhydrol.2005.07.003.
Iversen, C.M., 2010. Digging deeper: fine-root responses to rising atmospheric CO_2 concentration in forested ecosystems. New Phytol. 186 (2), 346–357. http://dx.doi.org/10.1111/j.1469-8137.2009.03122.x.
Jackson, R.B. et al., 1996. A global analysis of root distributions for terrestrial biomes. Oecologia 108 (3), 389–411.
Jarvis, N.J., 2011. Simple physics-based models of compensatory plant water uptake: concepts and eco-hydrological consequences. Hydrol. Earth Syst. Sci. 15, 3431–3446. http://dx.doi.org/10.5194/hess-15-3431-2011.
Jones, D.A., Wang, W., Fawcett, R., 2009. High-quality spatial climate data sets for Australia. Aust. Meteorol. Oceanogr. J. 58, 233–248.
Koster, R.D., Suarez, M.J., 1999. A simple framework for examining the interannual variability of land surface moisture fluxes. J. Climate 12 (7), 1911–1917.
Laio, F., Porporato, A., Ridolfi, L., Rodriguez-Iturbe, I., 2002. On the seasonal dynamics of mean soil moisture. J. Geophys. Res.-Atmos. 107 (D15). http://dx.doi.org/10.1029/2001JD001252.
McKenzie, N.J., Jacquier, D.W., Ashton, L.J., Cresswell, H.P., 2000. Estimation of Soil Properties Using the Atlas of Australian Soils. CSIRO Land and Water Technical Report 11/00. CSIRO, Canberra.
Milly, P.C.D., 1993. An analytic solution of the stochastic storage problem applicable to soil–water. Water Resour. Res. 29 (11), 3755–3758.
Milly, P.C.D., 1994a. Climate, interseasonal storage of soil–water, and the annual water-balance. Adv. Water Resour. 17 (1–2), 19–24.
Milly, P.C.D., 1994b. Climate, soil water storage, and the average annual water balance. Water Resour. Res. 30 (7), 2143–2156.
Milly, P.C.D., 2001. A minimalist probabilistic description of root zone soil water. Water Resour. Res. 37 (3), 457–463.
Northcote, K.H. et al., 1968. Atlas of Australian Soils, Sheets 1 to 10 with Explanatory Data. CSIRO and Melbourne University Press, Melbourne.
Oudin, L., Andreassian, V., Lerat, J., Michel, C., 2008. Has land cover a significant impact on mean annual streamflow? An international assessment using 1508 catchments. J. Hydrol. 357 (3–4), 303–316.
Palese, A.M., et al., 2000. The influence of soil water content on root density in young olive trees. In: Ferreira, M.I., Jones, H.G. (Eds.), Proceedings of the Third International Symposium on Irrigation of Horticultural Crops, Vols. 1 and 2. Acta Horticulturae. International Society Horticultural Science, Leuven 1, pp. 329–336.
Peel, M.C., Finlayson, B.L., McMahon, T.A., 2007. Updated world map of the Koppen–Geiger climate classification. Hydrol. Earth Syst. Sci. 11 (5), 1633–1644.
Peel, M.C., McMahon, T.A., Finlayson, B.L., 2010. Vegetation impact on mean annual evapotranspiration at a global catchment scale. Water Resour. Res. 46. http://dx.doi.org/10.1029/2009WR008233.
Penman, H.L., 1948. Natural evaporation from open water, bare soil and grass. Proc. Roy. Soc. Lond. A 193, 120–145.
Pink, B., 2008. Water and the Murray-Darling Basin: A Statistical Profile 2000-01 to 2005-06. Australian Bureau of Statistics, Canberra.
Polley, H.W., 1997. Implications of rising atmospheric carbon dioxide concentration for rangelands. J. Range Manage. 50 (6), 562–577.
Porporato, A., Daly, E., Rodriguez-Iturbe, I., 2004. Soil water balance and ecosystem response to climate change. Am. Nat. 164 (5), 625–632.
Potter, N.J., Zhang, L., 2009. Interannual variability of catchment water balance in Australia. J. Hydrol. 369 (1–2), 120–129.
Reich, P.B. et al., 2003. Variation in growth rate and ecophysiology among 34 grassland and savanna species under contrasting N supply: a test of functional group differences. New Phytol. 157 (3), 617–631.
Roderick, M.L., Farquhar, G.D., 2011. A simple framework for relating variations in runoff to variations in climatic conditions and catchment properties. Water Resour. Res. 47. http://dx.doi.org/10.1029/2010WR009826.
Rodriguez-Iturbe, I., Porporato, A., 2004. Ecohydrology of Water-controlled Ecosystems: Soil Moisture and Plant Dynamics. Cambridge University Press, Cambridge.
Rodriguez-Iturbe, I., Porporato, A., Laio, F., Ridolfi, L., 2001. Plants in water-controlled ecosystems: active role in hydrologic processes and response to water stress – I. Scope and general outline. Adv. Water Resour. 24 (7), 695–705.
Schenk, H.J., 2008. The shallowest possible water extraction profile: a null model for global root distributions. Vadose Zone J. 7 (3), 1119–1124. http://dx.doi.org/10.2136/vzj2007.0119.
Schenk, H.J., Jackson, R.B., 2002. Rooting depths, lateral root spreads and below-ground/above-ground allometries of plants in water-limited ecosystems. J. Ecol. 90, 480–494.
Schymanski, S.J., Sivapalan, M., Roderick, M.L., Beringer, J., Hutley, L.B., 2008. An optimality-based model of the coupled soil moisture and root dynamics. Hydrol. Earth Syst. Sci. 12 (3), 913–932.
Specht, R.L., 1972. Water use by perennial evergreen plant communities in Australia and Papua New Guinea. Aust. J. Bot. 20 (3), 273–299.
Stern, H., de Hoedt, G., Ernst, J., 2011. Objective classification of Australian climates. Bureau of Meteorology. <http://www.bom.gov.au/climate/environ/other/koppen_explain.shtml>.
Stone, E.L., Kalisz, P.J., 1991. On the maximum extent of tree roots. Forest Ecol. Manage. 46, 59–102.
Tjoelker, M.G., Craine, J.M., Wedin, D., Reich, P.B., Tilman, D., 2005. Linking leaf and root trait syndromes among 39 grassland and savannah species. New Phytol. 167 (2), 493–508. http://dx.doi.org/10.1111/j.1469-8137.2005.01428.x.
Trenberth, K.E., et al., 2007. Observations: Surface and Atmospheric Climate Change. In: S. Solomon et al. (Eds.), Climate Change 2007: The Physical Science Basis. Contribution of Working Group I to the Fourth Assessment Report of the Intergovernmental Panel on Climate Change. Cambridge University Press, Cambridge.
Yang, D.W., Sun, F.B., Liu, Z.T., Cong, Z.T., Lei, Z.D., 2006. Interpreting the complementary relationship in non-humid environments based on the Budyko and Penman hypotheses. Geophys. Res. Lett. 33 (18), L18402. http://dx.doi.org/10.1029/2006GL027657.
Yang, D.W. et al., 2007. Analyzing spatial and temporal variability of annual water-energy balance in nonhumid regions of China using the Budyko hypothesis. Water Resour. Res. 43 (4). http://dx.doi.org/10.1029/2006WR005224.
Yang, H.B., Yang, D.W., Lei, Z.D., Sun, F.B., 2008. New analytical derivation of the mean annual water-energy balance equation. Water Resour. Res. 44 (3). http://dx.doi.org/10.1029/2007WR006135.
Yang, D.W. et al., 2009. Impact of vegetation coverage on regional water balance in the nonhumid regions of China. Water Resour. Res. 45. http://dx.doi.org/10.1029/2008WR006948.
Zhang, L., Dawes, W.R., Walker, G.R., 2001. Response of mean annual evapotranspiration to vegetation changes at catchment scale. Water Resour. Res. 37 (3), 701–708.
Zhang, L. et al., 2004. A rational function approach for estimating mean annual evapotranspiration. Water Resour. Res. 40 (2), W02502. http://dx.doi.org/10.1029/2003WR002710.
Zhang, Y.Q., Viney, N., Chen, Y., Li, H.Y., 2011. Collation of streamflow data for 719 unregulated Australian catchments. Water for a Healthy Country National Research Flagship, CSIRO.